Direct observation of Hsp90-induced compaction in a protein chain

Mashaghi, Alireza; Moayed, Fatemeh; Koers, Eline J.; Zheng, Yang; Till, Katharina; Kramer, Günter; Mayer, Matthias P.; Tans, Sander J.

Important note
To cite this publication, please use the final published version (if applicable).
Please check the document version above.

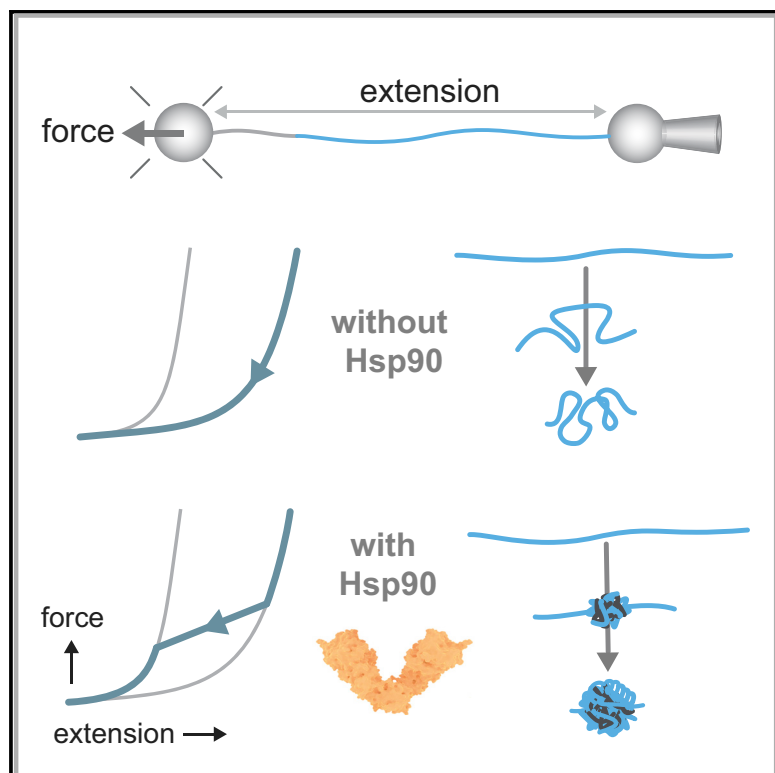# Direct observation of Hsp90-induced compaction in a protein chain

Graphical abstract

Authors

Alireza Mashaghi, Fatemeh Moayed, Eline J. Koers, ..., Günter Kramer, Matthias P. Mayer, Sander J. Tans

Correspondence

s.j.tans@tudelft.nl

In brief

By mechanically tethering individual protein clients at their termini with optical tweezers, Mashaghi et al. show that the chaperone Hsp90 can actively compact its unfolded substrates. This collapse-like process may have important consequences for folding and interactions with the Hsp70 system.

Highlights

- The Hsp90 chaperone can actively compact its client protein chains

- This induced compaction depends on ATP and performs mechanical work

- The Hsp90 interactions can suppress the formation of misfolded and aggregated structures

CellPress

Report

Direct observation of Hsp90-induced compaction in a protein chain

Alireza Mashaghi,[1,2,9] Fatemeh Moayed,[1,6,9] Eline J. Koers,[1,7,8,9] Yang Zheng,[3] Katharina Till,[1] Günter Kramer,[3,4] Matthias P. Mayer,[3] and Sander J. Tans[1,5,10,*]

[1]AMOLF, Amsterdam, the Netherlands
[2]Leiden Academic Centre for Drug Research, aculty of Science, Leiden University, Leiden, the Netherlands
[3]Center for Molecular Biology of Heidelberg University (ZMBH), DKFZ-ZMBH Alliance, Heidelberg, Germany
[4]German Cancer Research Center (DKFZ), Heidelberg, Germany
[5]Department of Bionanoscience, Kavli Institute of Nanoscience, Delft University of Technology, Delft, the Netherlands
[6]ASML, Veldhoven, the Netherlands
[7]Centre of Membrane Proteins and Receptors (COMPARE), University of Birmingham and University of Nottingham, Midlands, UK
[8]Division of Physiology, Pharmacology & Neuroscience, School of Life Sciences, University of Nottingham, Nottingham, UK
[9]These authors contributed equally
[10]Lead contact
*Correspondence: s.j.tans@tudelft.nl
https://doi.org/10.1016/j.celrep.2022.111734

SUMMARY

The chaperone heat shock protein 90 (Hsp90) is well known to undergo important conformational changes, which depend on nucleotide and substrate interactions. Conversely, how the conformations of its unstable and disordered substrates are affected by Hsp90 is difficult to address experimentally yet is central to its function. Here, using optical tweezers, we find that Hsp90 promotes local contractions in unfolded chains that drive their global compaction down to dimensions of folded states. This compaction has a gradual nature while showing small steps, is stimulated by ATP, and performs mechanical work against counteracting forces that expand the chain dimensions. The Hsp90 interactions suppress the formation of larger-scale folded, misfolded, and aggregated structures. The observations support a model in which Hsp90 alters client conformations directly by promoting local intra-chain interactions while suppressing distant ones. We conjecture that chain compaction may be central to how Hsp90 protects unstable clients and cooperates with Hsp70.

INTRODUCTION

The heat shock protein 90 (Hsp90) chaperone is highly conserved and essential in eukaryotic cells. It is involved in many cellular functions, ranging from protection against heat stress to signal transduction and protein trafficking (Taipale et al., 2010), which often involve cooperation with Hsp70 (Genest et al., 2011; Kirschke et al., 2014). Hsp90 interacts with many co-chaperones in eukaryotes (Echeverria et al., 2011; Mayer and Le Breton, 2015), whereas no co-chaperone has been identified for the *Escherichia coli* Hsp90, also termed HtpG. Hsp90 undergoes large conformational changes during its ATPase cycle (Figure 1A) (Krukenberg et al., 2009; Shiau et al., 2006; Street et al., 2011). Hsp90 interacts preferentially with unstable disordered regions (Schneider et al., 1996). The intrinsically disordered Tau bound an open state of Hsp90 in an ATP-independent manner, whereas ATP did affect the Hsp90 state of pre-formed Tau-Hsp90 complexes (Karagoz et al., 2014). The disordered ribosomal protein L2 accelerated ATP hydrolysis by Hsp90, suggesting it stimulates Hsp90 closure (Motojima-Miyazaki et al., 2010). HtpG bound a locally structured region of the partially folded Δ131Δ (Street et al., 2014), while Hsp90 bound the glucocorticoid

receptor in open and closed states (Lorenz et al., 2014). In contrast to Δ131Δ and L2, however, binding here slowed Hsp90 closure and decelerated ATP hydrolysis. Overall, these findings indicate that substrate binding affects and depends on Hsp90 conformation.

In contrast, it remains poorly understood how Hsp90 affects substrate conformations. Bacterial Hsp90 requires cooperation with Hsp70 to aid refolding (Genest et al., 2011; Moran Luengo et al., 2018). Hsp90 can reactivate luciferase with Hop/Sti1 (Johnson et al., 1998) and modulate the activity of steroid receptors with Hsp70 and co-chaperones (Morishima et al., 2000). Hsp90 can facilitate *de novo* folding in the cell, where various additional factors are present (Thomas and Baneyx, 2000). How unfolded protein chains are affected by Hsp90 (or HtpG) alone is incompletely resolved (Street et al., 2014). Addressing this issue is technically challenging. The disordered nature of Hsp90 substrates suggests that during their interaction with Hsp90, they may be characterized by conformational ensembles rather than distinct conformational states. Moreover, the diverse possible binding sites on Hsp90 indicate the possibility of additional conformational heterogeneity and dynamics that are difficult to characterize.
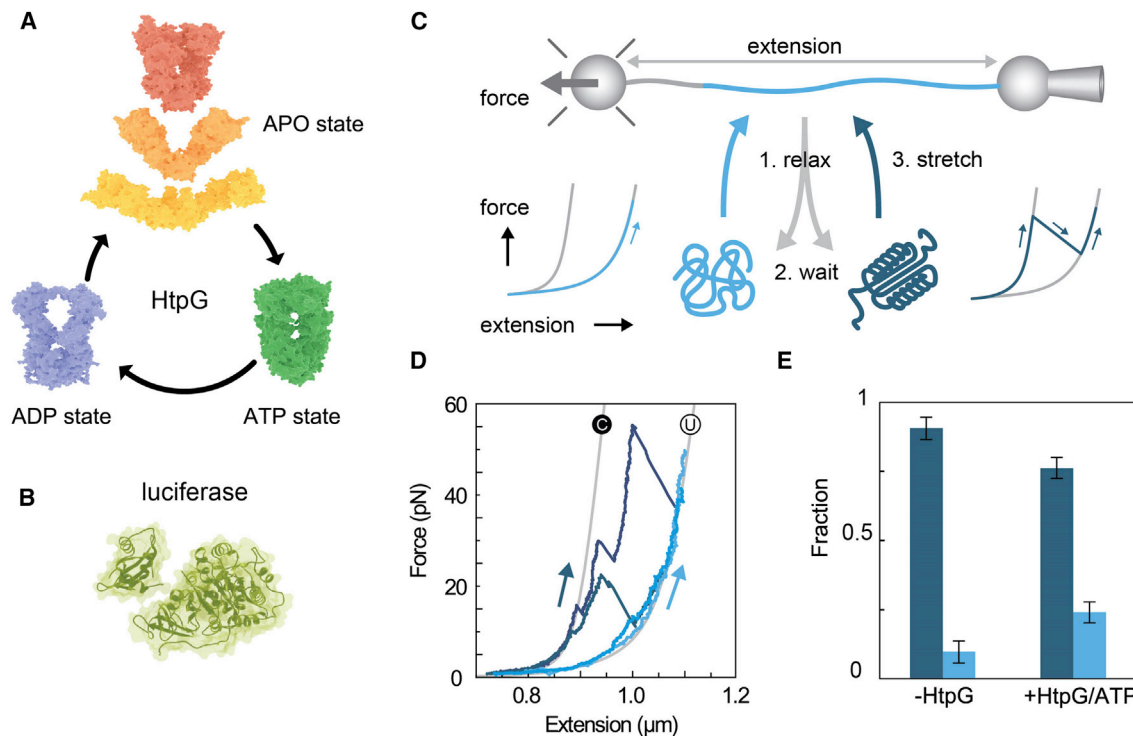
Figure 1. HtpG stabilizes the unfolded state of luciferase
(A) Possible conformations assumed by bacterial Hsp90 (HtpG) when progressing through its ATPase cycle, ADP state PDB: 2IOP (Shiau et al., 2006), ATP state
(*S. cerevisiae*) PDB: 2CG9 (Ali et al., 2006), APO states middle: PDB: 2IOQ (Shiau et al., 2006), and APO states top and bottom (Krukenberg et al., 2009).
(B) Firefly luciferase structure PDB: 1LCY (Conti et al., 1996).
(C) Schematic diagram of assay to measure stabilization of unfolded state. Luciferase is tethered between two beads using DNA linkers and fully unfolded and
extended (top), then relaxed to 0 pN for 5 s. Subsequent stretching shows that the chain has remained unfolded (right, light blue) or adopted tertiary structure, as
shown by an initially more compact state that unfolds in discrete steps (left, dark blue). Measured traces are shown in (D), and the fractions of these two cases in (E).
(D) Stretching traces, taken from cycles as described in (C), showing the chain remained unfolded (light blue) or adopted tertiary structure (dark blue).
(E) Fraction of cycles showing protein chain remained unfolded (light blue) or adopted tertiary structure (dark blue). See (C) for description. Conditions are no HtpG
(n = 53 cycles), and 1 μM HtpG with 1 mM ATP (n = 126 cycles). Error bars are SEM. See STAR Methods for details.

Here, we study this issue by manipulating individual Firefly luciferase molecules, as well as maltose-binding protein (MBP) and the glucocorticoid receptor, using optical tweezers. We aim to study how interactions with bacterial Hsp90 (HtpG) locally affect the conformation of unfolded substrates rather than how Hsp90 assists in folding, which involves Hsp70 and other co-factors. Local structures that form in unfolded chains and hence change the distance between the N and C termini can be followed using optical tweezers, even if transient and heterogeneous. Our experiments showed HtpG can produce a gradual compaction in unfolded luciferase, and sudden stepwise contractions, in an ATP-stimulated manner. HtpG was found to suppress entry into a kinetically trapped state (luciferase) and aggregation between proteins (MBP). The data indicate that HtpG promotes local intra-chain contacts within client protein chains while suppressing distant contacts and induces a spectrum of transiently stable local conformations and overall chain compaction. This function may also have important implications for the interplay between Hsp90 and Hsp70 (Kirschke et al., 2014; Rodriguez et al., 2008; Sharma et al., 2010). More generally, protein chain compaction or collapse is key to protein states including phase separation

(Dill, 1985; Kim and Baldwin, 1982) and may be broadly relevant to protein quality control.

RESULTS

Stabilization of the unfolded state by Hsp90
We surmised that one effect of Hsp90 could be the stabilization of unfolded substrate states, as the ability of Hsp90 to bind unfolded regions can compete with tertiary structure formation in the polypeptide chain. To investigate such stabilization of unfolded states by bacterial Hsp90 (HtpG) at the single-molecule level, we tethered a luciferase protein (Figure 1B) between two polystyrene beads via a DNA linker and unfolded it fully by mechanical stretching (Figure 1C). In these experiments, we continuously measure the distance between the beads, also referred to as the extension, as well as the force within the protein-DNA tether. Next, we relaxed the unfolded chain, waited at 0 pN for 5 s, and then stretched to assess whether it had remained unfolded or had formed tertiary structure (Mashaghi et al., 2014). For unfolded chains, stretching traces follow approximately a force-extension curve for a non-interacting polypeptide chain (of the length of luciferase) tethered to DNA, which is well

predicted by the worm-like chain (WLC) model (Figure 1D, light blue traces) (Marko and Siggia, 1995). For chains with tertiary structure, the stretching data initially display compact conformations, which subsequently show discrete unfolding transitions (Figure 1D, dark blue traces). In the absence of HtpG, we found that in 9% of the relaxation-stretching cycles, the chain remained in or near the unfolded state (Figure 1E, light blue bar). In the presence of HtpG and ATP, the first stretching curves for newly tethered luciferase proteins were similar to the curves without HtpG, indicating a lack of interaction. After full unfolding, we similarly continued with cycles of relaxation, waiting at 0 pN for 5 s, and stretching. Now, a larger fraction (24%, $p < 0.05$, Figure 1E, light blue bar) of the cycles showed that the chain remained in or near the unfolded state. These observations suggested that HtpG bound the unfolded chains, which is consistent with previous reports (Karagoz et al., 2014; Street et al., 2011), and can hence stabilize the unfolded state.

Protein chain compaction by Hsp90

The relaxation data showed another type of effect on the unfolded luciferase substrates. Theory indicates that during relaxation to low force, an extended non-interacting protein chain coils up as described by the WLC force-extension curve (Figure 2A, blue curve). Unfolded luciferase chains without HtpG present typically displayed that behavior while showing deviations at lower forces (Figure 2B, below 5 pN). In presence of HtpG and ATP, relaxation data deviated more strongly, with chains compacting when the force decreased below 25 pN, as indicated by extensions smaller than the unfolded-chain WLC model. We observed chains that became similarly compact as fully folded states for forces below a few pN, with force-extension data following the WLC model for the folded state (Figures 2C and 2D). The compaction progressed gradually with decreasing force while displaying small stepwise contractions down to the resolution limit of about 10 nm (Figure 2D). Overall, these data indicated a gradual compaction of the protein chain.

To quantify the compaction effects, we determined the surface area under the relaxation traces (Figure 2E). We are interested in deviations from a non-interacting chain, and hence we subtracted the area corresponding WLC behavior, as well as that of the DNA linker (STAR Methods). Note that this surface area reflects mechanical work. Here, we refer to it as the "relaxation energy," but note that it does not signify an equilibrium (free) energy. For the relaxation traces of luciferase without HtpG, this analysis showed a small, but non-zero, relaxation energy that extended up to 250 k_BT (Figure 2E, light blue). The order of magnitude of these effects are consistent with previous atomic force microscopy pulling studies of the hydrophobic collapse of isolated protein chains (Walther et al., 2007). In line with the observed compaction, the distribution of the relaxation energy increased with HtpG, and ATP now extended to 600 k_BT (Figure 2E, dark blue). Thus, HtpG induced contractions in the protein chain against a counter-acting force.

Next, we tested whether human Hsp90 (hHsp90) also induced chain compactions in one of its clients, the glucocorticoid receptor ligand-binding domain (GRLBD). We found relaxation energies that were predominantly below 15 k_BT in the absence of

hHsp90 (Figure S1). In the presence of hHsp90 and ATP, the relaxation energies were predominantly above 15 k_BT, and the histogram now displayed a shoulder extending up to 75 k_BT (Figure S1). Thus, hHsp90 promoted a contraction in the GR chain despite the counter-acting forces acting within it. Overall, these data indicated that both bacterial and hHsp90 can compact protein chains.

Hsp90 lowers the kinetic barrier to compacted states

In addition to the area under the relaxation trace, which estimates the compaction energy, one may also quantify the area under the stretching traces (Figure 2F). For luciferase, this stretching energy was found to decrease on average in the presence of HtpG (Figure 2G; $p < 0.05$). Thus, whereas HtpG increased the relaxation energy, it decreased the stretching energy. These opposing trends indicated that the resulting compacted chain conformations, which are possibly complexed with HtpG, are less resistant to force than the folded conformations in the absence of HtpG. The gradual compaction was also found to display small local steps, which likely involve few residues that are close together along the protein chain. In contrast, larger global folding transitions often involve many residues that may be far apart along the protein chain.

The notion of hysteresis can help to further discuss and explain this point. In general, hysteresis informs on the history dependence of a system. A system is non-hysteretic when its current state does not depend on its previous state. For example, for a theoretical non-interacting chain undergoing relaxation-stretching cycles, the measured extension depends on the currently applied force as given by the WLC model but not on previously applied forces. In such cases, the relaxation and stretching curves overlap, and the relaxation and stretching energies are identical. A different situation arises when considering (un)folding, for instance. As the tension is increased to a certain force, a chain that was folded may remain folded, but when the tension is decreased to that same force, the chain that was unfolded may remain unfolded. The delay in (un)folding is relevant here: both processes take time, which preserves previous states. The system is then not in thermodynamic equilibrium, and the difference in relaxation and stretching energies indicates the hysteresis. A limited hysteresis typically indicates low kinetic folding barriers and hence fast folding, as observed for small folds that exhibit limited cooperativity between residue-residue contacts (Jagannathan and Marqusee, 2013). Conversely, larger tertiary structures with complex folds and many cooperative contacts tend to exhibit large kinetic barriers, slow folding, and significant hysteresis (Shank et al., 2010).

Here, we determine the hysteresis by the difference between the relaxation and stretching energies of each relax-stretch cycle, as assessed by plotting one against the other (Figure 2H). The distance from the diagonal then quantifies the hysteresis. In the absence of HtpG, the cycles typically were separated from the diagonal by a distance of order 100 k_BT, which indicated substantial hysteresis, and is expected for a chain that folds (Figure 2H, light blue points). In the presence of HtpG and ATP, some cycles also displayed hysteresis, but many points were now close or on the diagonal, indicating limited to no hysteresis (Figure 2H, dark blue points). The
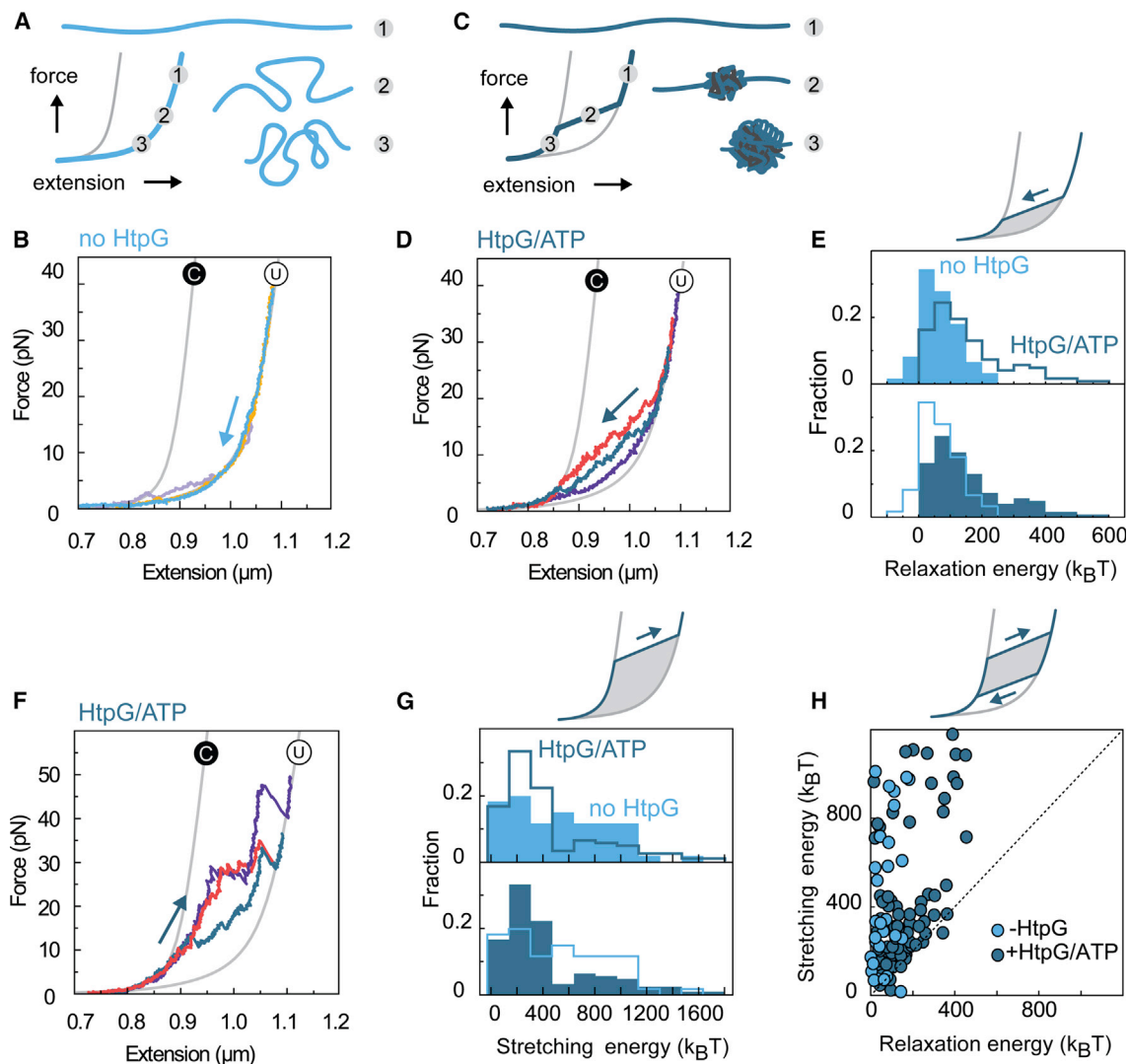
Figure 2. HtpG compacts unfolded luciferase chains

(A) Cartoons of a non-interacting chain that coils up when the force is decreased from 1 to 3, and corresponding force-extension curve.

(B) Measured force-extension data for unfolded luciferase that is relaxed from high to low force, from different relax-stretch cycles and different molecules.

(C) Cartoons of a chain that collapses to a compact state when the force is decreased from 1 to 3, and corresponding force-extension curve.

(D) Measured force-extension data for unfolded luciferase that is relaxed from high to low force in presence of HtpG and ATP, from different relax-stretch cycles and different molecules.

(E) Histogram of observed relaxation energies in the absence (light blue, n = 63 traces) and presence of HtpG and ATP (dark blue, n = 125 traces), as quantified by the surface area in between the relaxation trace and the theoretical worm-like chain model (top).

(F) Measured stretching data from low to high force in presence of HtpG and ATP, from different relax-stretch cycles and different molecules.

(G) Histogram of stretching energy, in the absence (light blue, n = 63 traces) and presence of HtpG and ATP (dark blue, n = 125 traces) as quantified by the surface area in between the stretching trace and the theoretical worm-like chain model (top).

(H) Hysteresis quantification. Relaxation energy against the stretching energy of the subsequent stretching trace. Distance from the diagonal quantifies the hysteresis of the cycle. Points on the diagonal reflect a lack of hysteresis.

See also Figure S1.

relaxation (and stretching) energies were up to 400 k_BT in these non-hysteretic cycles. Thus, while the resulting states were compacted like folded states, they displayed a lack of hysteresis. Such reversibility has been observed in the formation and disruption of collapsed states in individual hydrophobic polymers (Li and Walker, 2011). Note that the relaxation process takes 10 s and shows limited compaction without

HtpG, while significant compaction occurs in the 5 s folding window. These observations and associated hysteresis are consistent with luciferase folding being efficiently suppressed by the applied force, which is present during relaxation but not during the folding time window. Conversely, the limited hysteresis in the presence of HtpG is consistent with the compaction steps being smaller; their formation can take place at higher
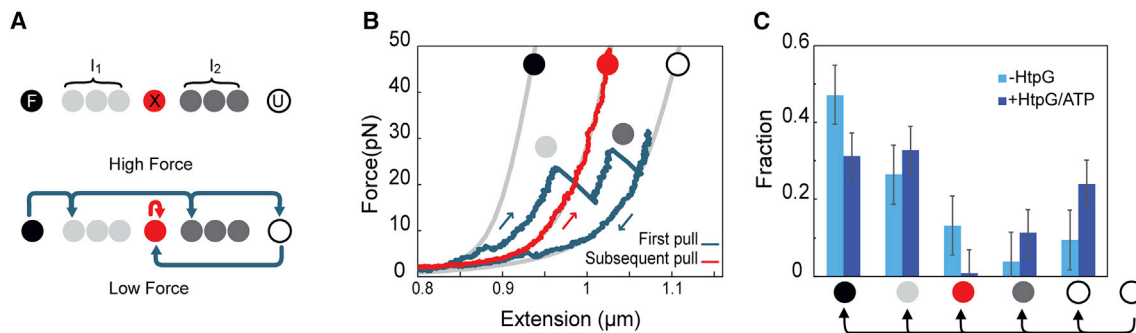
Figure 3. Misfold suppression by HtpG

(A) Schematic representation of observed Firefly luciferase states ordered by protein length, ranging from fully compact (F; black) to fully unfolded (U; white) state (top panel). Also indicated are a misfolded state (X; red), and states that are more compact (I_1; light gray) or less compact (I_2; dark gray). Bottom panel: transitions between states observed in (B) during stretching (top arrows) and in relaxed states (bottom arrows).

(B) Stretching and relaxation (blue traces), waiting at 0 pN for 5s, and stretching (red trace). Data show entry into state (X, red) of about 105 nm, which is stable over minutes and resists high forces, and corresponds to a misfolded state (Mashaghi et al., 2014). Gray lines are worm-like chain theoretical predictions of F and U states.

(C) Corresponding fraction of observed entry into the different states indicated in (A), in the absence (light blue, n = 53 cycles) and presence (dark blue, n = 126 cycles) of bacterial Hsp90 (HtpG, 1 μM). Cycles consist of relaxing chains in the fully unfolded state (right-most white circle), followed by a 5 s waiting time at 0 pN that provides an opportunity to adopt a different folded state. The latter is quantified in subsequent stretching, as illustrated in (B). The data show that HtpG suppresses entry into state X more strongly than the other states. Error bars represent the standard error calculated by assuming each population is independent. See also Figure S2.

applied force, while their disruption occurs at lower forces (compared with the no-chaperone case). Taken together, the decrease of hysteresis in the presence of HtpG suggests that Hsp90 lowers the kinetic barrier to compacted states.

Suppression of misfolding by HtpG

The data so far indicated that HtpG can promote the formation of compacted structures of dimensions down to a similar order as fully folded states, within the measurement limits of our experiments. This compaction was gradual and displayed small steps (Figure 2D). Consistent with the reversibility observed in the previous section, the stretching traces also displayed similar gradual and small step features Figure 2F) and were hence distinct from the stretching traces in the absence of HtpG (Figure 1D, dark blue traces). Note that some stretching traces also showed the larger steps that were common in the absence of HtpG (Figures 2D and 1D), which may indicate that the luciferase polypeptides are not affected everywhere by HtpG and hence allows partial refolding of luciferase. These data are also consistent with previous bulk data showing that HtpG alone does not refold luciferase and rather requires cooperation with DnaK (Moran Luengo et al., 2018).

A related issue is if Hsp90 affects entry into kinetically trapped misfolded states along the folding pathway. Luciferase is known to adopt non-native states by repeated freeze-thaw cycles (Genest et al., 2011; Johnson et al., 1998). Luciferase has also been shown to adopt kinetically trapped states in mechanical relaxation-stretching cycles (Mashaghi et al., 2014). During the 5 s waiting time at 0 pN in stretching and relaxation cycles, and in the absence of chaperone, luciferase indeed formed compact structures, termed X states, that are characterized by a protein length (the length of the unstructured part of the protein) of about 105 nm (13% of the cycles; Figures 3A and 3B, red state). These states can be distinguished from larger (I1) and smaller (I2) inter-

mediate structures (Figures 3A and 3B). These X states have been identified as kinetically trapped misfolded states as they have a significantly longer lifetime (minutes) and a maximally sustained force (43 pN on average) that is larger than other states of intermediate size (seconds and 24 pN, respectively) (Mashaghi et al., 2014). This maximally sustained force equals the unfolding force when unfolding occurs or the largest measured force when unfolding does not occur during stretching. In the presence of HtpG and ATP, the formation of misfolded X-state structures was almost abolished: their frequency was reduced more than 10-fold (from 13% to 0.8% of the cycles, p < 0.05; Figure 3C). The other folded states, including I1 and I2, did not show such a significant decrease (Figure 3C). Overall, the data indicated that HtpG suppressed luciferase misfolding.

To further probe these issues, we performed bulk assays in which luciferase is diluted from a chemically denatured state in a refolding buffer and luciferase luminescence is measured (Figures S3C–S3E). We found weak luminescence for luciferase only, indicating its tendency to misfold and aggregate (Figure S3D). The presence of HtpG led to a significant, yet small, increase in luminescence (Figure S3D). This finding is consistent with the single-molecule results, which showed that HtpG can suppress misfolding (Figure 3) and aggregation interactions (Figure S2), and stabilize the unfolded state (Figure 1E). Care must be taken in these comparisons, however, due to the key differences between the assays. Consistent with previous work (Genest et al., 2011; Moran Luengo et al., 2018), we found that adding the DnaK/Hsp70 system improved the yield significantly (Figure S3E). There was no significant difference between the yields with or without ATP, consistent with our single-molecule refolding assay results (Figure 4C).

To assess whether this misfold suppression by HtpG could occur beyond luciferase, we considered a different protein system. We focused on a construct composed of four MBP
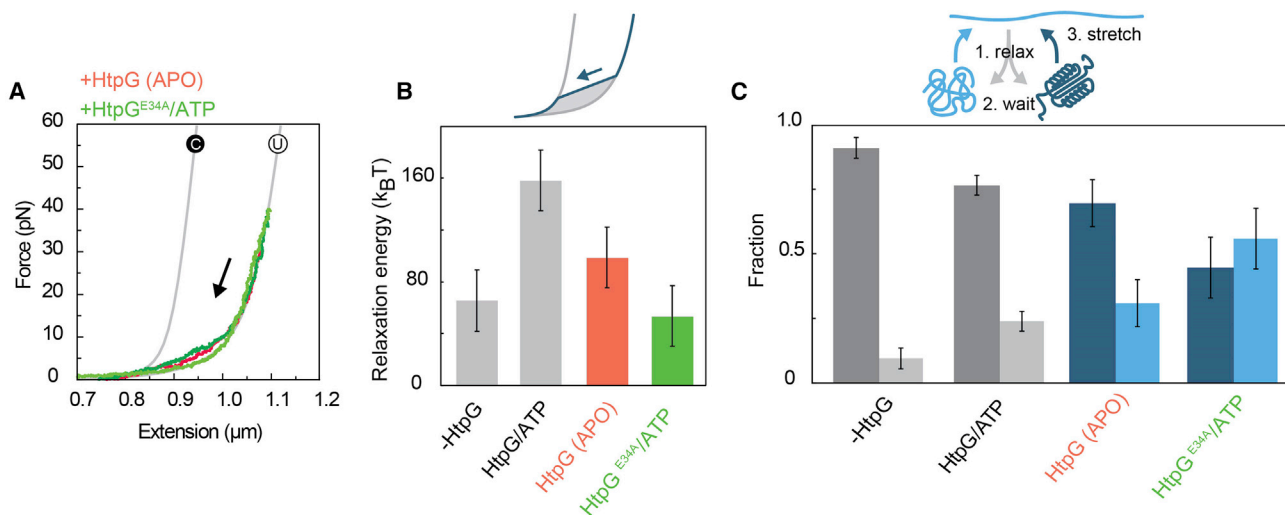
Figure 4. HtpG-promoted luciferase conformational changes are stimulated by ATP hydrolysis
(A) Relaxation traces with bacterial Hsp90 (HtpG, 1μM) and no ATP or HtpG-E34A with ATP.
(B) Analysis of relaxation energy in the presence of HtpG/ATP (n = 125 traces), HtpG (APO, n = 29 traces), no chaperone (n = 63 traces), and HtpG^{E34A}/ATP (n = 18 traces; supplemental information), error bars are SEM.
(C) Fraction of relaxation-stretching cycles that either did (dark blue) or did not (light blue) show the formation of tertiary structure (during relaxation and waiting at 0 pN for 5 s), with the formation of structure evidenced by discrete unfolding steps during subsequent stretching. Definitions as in Figure 1E; no HtpG (n = 53 cycles), HtpG/ATP (n = 126 cycles), HtpG (APO, n = 26 cycles), and HtpGE34A/ATP (n = 18 traces), error bars are SEM.
See also Figure S3.

monomers arranged head to tail (4MBP), which has been used as a model system for protein misfolding and aggregation (Bechtluft et al., 2007; Mashaghi et al., 2013). Stretching this 4MBP construct for the first time in the absence of HtpG results in an unfolding pattern that is characterized by four discrete events reflecting the unfolding of four MBP core structures (Figures S2A and S2B). As shown previously (Bechtluft et al., 2007; Mashaghi et al., 2013), after relaxation and waiting at 0 pN for 5 s, we observed compact structures that often could not be unfolded fully (Figure S2C). The traces also showed steps larger than one MBP core, which thus indicated structures involving more than one MBP core (Figures S2C and S2E). Together, these data indicated misfolding due to non-native contacts between different MBP cores. In the presence of HtpG and ATP, we found that the first stretching trace was similar to that without HtpG, thus mirroring the lack of interaction in the first luciferase stretching traces. Subsequent stretching traces now were quite different. Tight misfolds that could not be unfolded were only rarely observed (Figures S2D and S2E). Moreover, we now observed the discrete events reflecting the unfolding of precisely one MBP core (Figure S2D). The presence of HtpG led to an about 3-fold increase of such events (Figure S2E; from 4% to 13%, p < 0.05). Overall, these data suggested that HtpG suppressed global misfolding interactions between different cores while still allowing local interactions within single cores required for their refolding.

Conformational changes promoted by HtpG are stimulated by ATP hydrolysis

HtpG undergoes conformational changes driven by an ATP hydrolysis cycle (Figure 1A), which raises the question of whether the observed effects depend upon it or not. In experiments with HtpG but without ATP (HtpG-APO), we found that the area under luciferase relaxation traces (Figure 4A) was on average smaller than with HtpG and ATP (Figure 4B; p < 0.05), indicating that HtpG-mediated compaction was stimulated by ATP presence. We found that for HtpG-APO, the fraction of cycles where the chain remained in or near the fully unfolded state (31%; Figure 4C) was about equal to that for HtpG-ATP (24%) and hence was higher than in the absence of HtpG (9%), consistent with HtpG-APO interacting with the luciferase chain.

Next, we aimed to probe the role of ATP hydrolysis. ATP hydrolysis in Hsp90 proteins occurs within a conserved ATP-binding site (Prodromou et al., 1997). In HtpG, a Glu-to-Ala mutation at residue 34 in this binding site decreases the rate of ATP hydrolysis about 10-fold and is considered less ambiguous than non-hydrolysable ATP analogs (Genest et al., 2011; Graf et al., 2009). In the presence of HtpG^{E34A} and ATP, the stabilization of the unfolded state was most efficient, with 55% of cycles maintaining the chain in or near the fully unfolded state (Figure 4C). These findings indicated that HtpG^{E34A} bound the unfolded luciferase. However, relaxation traces in the presence of HtpG^{E34A} displayed a low relaxation energy (Figures 4A and 4B) and hence lacked the compaction that was seen for wild-type (WT) HtpG-ATP. These data indicated that HtpG^{E34A} with ATP interacted with the unfolded luciferase chain but did not promote compaction.

We also observed a lack of compaction by WT HtpG and ATP in the presence of Radicicol (Figures S3A and S3B), which is consistent with its ATPase-inhibitory role. Overall, the data thus indicated that ATP hydrolysis stimulated HtpG-promoted compaction. We do note that for compaction of GRLBD by

hHsp90, we did not find a stimulatory effect of ATP but rather a small decrease in the relaxation energy from 42 k_BT in the absence of ATP (Figure S1E) to 25 k_BT in the presence of ATP (Figure S1A). Such differences in ATP dependence between HtpG and hHsp90 could be due to many factors and may, for instance, be related to the stronger coupling of conformational change and the ATP cycle (Graf et al., 2014; Mickler et al., 2009; Ratzke et al., 2012), the client in question, or the absence of co-chaperones like Sti1/hop and p23 in the case of hHsp90.

DISCUSSION

Our data show that bacterial Hsp90 (HtpG) can induce a global compaction of extended client chains driven by local contractions. More specifically, (1) HtpG can trap substrates in states without significant stable tertiary structure or low contact order (Figure 1E), which suggests binding to extended segments or other small structures of marginal stability. (2) The global compaction driven by local contractions (Figures 2D and 2E) imply forces that drive it, which can overcome opposing forces that promote chain expansion and may originate from chain entropy and delay folding (Dill, 1985). (3) ATP hydrolysis suppression abolished the stimulated compaction (Figures 4A and 4B) but yielded efficient stabilization of low-contact-order states (Figure 4C). For yeast Hsp90, ATP hydrolysis was not essential for cellular viability, though the growth rate was reduced (Zierer et al., 2016). Differences between bacterial and yeast Hsp90 could be related to the tighter conformational control by ATP in the former (Mickler et al., 2009; Ratzke et al., 2012), may reflect compensatory effects by other chaperones *in vivo*, or may indicate that eukaryotic Hsp90 needs co-chaperones. (4) Hsp90 suppressed entry into misfolded and aggregated states (Figure 3C), which can be toxic to cells. These findings are consistent with increased aggregation in heat-shocked ΔHsp90 cells (Thomas and Baneyx, 2000) and the suppression of heat-activated aggregation by Hsp90 (Jakob et al., 1995).

The observed gradual compaction, including its reversibility and lack of hysteresis, indicates a spectrum of heterogeneous and transiently stable local conformations with low kinetic barriers. Binding to the open followed by the closed HtpG conformation (Figure 1A) may promote substrate compaction. The substrate may also fluctuate between more and less compact, with HtpG stabilizing the former. The promotion of local compact conformations, which is consistent with previous work (Street et al., 2014), may underlie the misfolding suppression seen here. Hsp90 may shield these local structures from interactions with other segments, which are distant, most likely part of different domains, and hence can produce non-native structures. Indeed, interactions between domains are considered a general factor contributing to misfolding (Han et al., 2007; Tian and Best, 2016).

A similar model was proposed by us for trigger factor (Mashaghi et al., 2013; Singhal et al., 2015). Differences are also notable. The HtpG-induced compaction was more heterogeneous and gradual than for trigger factor, which implies that the substrate conformers are smaller. Optical tweezer studies showed that DnaK/Hsp70, Hsp33, and Hsp26 also interact with compact conformations, which were typically near native, besides binding

unfolded states (Mashaghi et al., 2016; Moayed et al., 2020; Ungelenk et al., 2016). This binding of partially folded structures contrasts with the observed behavior of SecB and DnaJ, which also suppress aggregation but by stabilizing unfolded states exclusively instead (Bechtluft et al., 2007; Mashaghi et al., 2016; Perales-Calvo et al., 2018). While a force-generating compaction was not detected for either of these chaperones, a similar effect was recently reported by us for GroEL where it played a role in triggering folding (Naqvi et al., 2022). Unfolded substrates in molten-globule-like states in complex with chaperones have been detected by nuclear magnetic resonance (NMR) (Hiller, 2019), as well as their folding (Stull et al., 2016). These results raise further questions on the dynamic basis of chaperone function. The Hsp90-induced compaction may, for instance, help explain transfer from Hsp70 to Hsp90. Hsp90 could counteract Hsp70 binding and associated local unfolding. These processes may play roles in signal transduction pathways (Kirschke et al., 2014; Mashaghi et al., 2016; Rodriguez et al., 2008; Sharma et al., 2010).

In summary, our study provides a direct observation of unfolded protein chains as they interact with Hsp90. The observed chain compaction impacts our understanding of how Hsp90 affects the formation and stability of tertiary structures and its cooperation with other chaperone systems. We speculate that Hsp90 has more direct role in altering the structure of its kinase and receptor clients beyond binding disordered regions and suppressing structure formation.

Limitations of the study
Our results indicate that Hsp90 not only interacts with its unfolded clients but also promotes their compaction and suppresses their misfolding and aggregation. These findings suggest that Hsp90 induces a local conformation within the client polypeptide and may complex with these local conformers, either transiently or in a stable manner. While our method can detect the occurrence of the associated client contractions, it unfortunately cannot provide structural information on these complexes, which would be important to understand the detailed molecular basis. Another open question concerns the molecular basis of the ATP dependence. At this point, it is unclear how ATP hydrolysis, Hsp90 conformational change, and client conformational change are related and ordered in time. To address these issues, it would be important to elucidate which specific client segments or sequences interact most strongly with Hsp90 in this compaction binding mode such that more detailed and focused study can be performed. It will also be important to study how interaction between Hsp90 and the Hsp70 system, as well as co-chaperones, alters the observed compaction and contributes to folding and regulatory functions of Hsp90 and Hsp70.

STAR★METHODS

Detailed methods are provided in the online version of this paper and include the following:

- KEY RESOURCES TABLE
- RESOURCE AVAILABILITY

SUPPLEMENTAL INFORMATION

Supplemental information can be found online at https://doi.org/10.1016/j.celrep.2022.111734.

AUTHOR CONTRIBUTIONS

A.M., F.M., E.J.K., M.P.M., G.K., and S.J.T. conceived and designed the research; G.K. designed and purified the MBP and luciferase protein constructs and the bacterial Hsp90; M.P.M. supplied the hHsp90; E.J.K. designed and purified the GRLBD-DNA chimera; A.M., F.M., E.J.K., and K.T. performed the optical tweezers experiments; G.K. and M.P.M. supplied the chaperones; Y.Z. performed the luciferase refolding assays; A.M., F.M., E.J.K., and S.J.T. analyzed the data; and F.M., A.M., E.J.K., M.P.M., G.K., and S.J.T. wrote the paper. Work in the group of M.P.M. was supported by DFG project ID 422001793 (MA1278/7-1).

DECLARATION OF INTERESTS

The authors declare no competing interests.

REFERENCES

Ali, M.M.U., Roe, S.M., Vaughan, C.K., Meyer, P., Panaretou, B., Piper, P.W., Prodromou, C., and Pearl, L.H. (2006). Crystal structure of an Hsp90-nucleotide-p23/Sba1 closed chaperone complex. Nature *440*, 1013–1017.

Andreasson, C., Fiaux, J., Rampelt, H., Mayer, M.P., and Bukau, B. (2008). Hsp110 is a nucleotide-activated exchange factor for Hsp70. J. Biol. Chem. *283*, 8877–8884.

Antos, J.M., Ingram, J., Fang, T., Pishesha, N., Truttmann, M.C., and Ploegh, H.L. (2017). Site-specific protein labeling via sortase-mediated transpeptidation. Current Protocols in Protein Science *Chapter 15*. 15.13.

Bechtluft, P., van Leeuwen, R.G., Tyreman, M., Tomkiewicz, D., Nouwen, N., Tepper, H.L., Driessen, A.J., and Tans, S.J. (2007). Direct observation of chaperone-induced changes in a protein folding pathway. Science *318*, 1458–1461.

Beckett, D., Kovaleva, E., and Schatz, P.J. (2008). A minimal peptide substrate in biotin holoenzyme synthetase-catalyzed biotinylation. Protein Sci. *8*, 921–929.

Conti, E., Franks, N.P., and Brick, P. (1996). Crystal structure of firefly luciferase throws light on a super-family of adenylate-forming enzymes. Structure *4*, 287–298.

Dill, K.A. (1985). Theory for the folding and stability of globular proteins. Biochemistry *24*, 1501–1509.

Echeverria, P.C., Bernthaler, A., Dupuis, P., Mayer, B., and Picard, D. (2011). An interaction network predicted from public data as a discovery tool: application to the Hsp90 molecular chaperone machine. PLoS One *6*.

Genest, O., Hoskins, J.R., Camberg, J.L., Doyle, S.M., and Wickner, S. (2011). Heat shock protein 90 from Escherichia coli collaborates with the DnaK chaperone system in client protein remodeling. Prod. Natl. Acad. Sci. USA *108*, 8206–8211.

Gittes, F., and Schmidt, C.F. (1998). Interference model for back-focal-plane displacement detection in optical tweezers. Opt Lett. *23*, 7–9.

Graf, C., Lee, C.-T., Eva Meier-Andrejszki, L., Nguyen, M.T.N., and Mayer, M.P. (2014). Differences in conformational dynamics within the Hsp90 chaperone family reveal mechanistic insights. Front. Mol. Biosci. *1*.

Graf, C., Stankiewicz, M., Kramer, G., and Mayer, M.P. (2009). Spatially and kinetically resolved changes in the conformational dynamics of the Hsp90 chaperone machine. Embo J *28*, 602–613.

Han, J.H., Batey, S., Nickson, A.A., Teichmann, S.A., and Clarke, J. (2007). The folding and evolution of multidomain proteins. Nat. Rev. Mol. Cell Biol. *8*, 319–330.

Hiller, S. (2019). Chaperone-bound clients: the importance of being dynamic. Trends Biochem. Sci. *44*, 517–527.

Jagannathan, B., and Marqusee, S. (2013). Protein folding and unfolding under force. Biopolymers *99*, 860–869.

Jakob, U., Lilie, H., Meyer, I., and Buchner, J. (1995). Transient interaction of Hsp90 with early unfolding intermediates of citrate synthase. Implications for heat shock in vivo. J. Biol. Chem. *270*, 7288–7294.

Johnson, B.D., Schumacher, R.J., Ross, E.D., and Toft, D.O. (1998). Hop modulates hsp70/hsp90 interactions in protein folding. J. Biol. Chem. *273*, 3679–3686.

Kalia, J., and Raines, R.T. (2007). Catalysis of imido group hydrolysis in a maleimide conjugate. Bioorg. Med. Chem. Lett. *17*, 6286–6289.

Karagoz, G.E., Duarte, A.M.S., Akoury, E., Ippel, H., Biernat, J., Luengo, T.M., Radli, M., Didenko, T., Nordhues, B.A., Veprintsev, D.B., et al. (2014). Hsp90-Tau complex reveals molecular basis for specificity in chaperone action. Cell *156*, 963–974.

Kim, P.S., and Baldwin, R.L. (1982). Specific intermediates in the folding reactions of small proteins and the mechanism of protein folding. Annu. Rev. Biochem. *51*, 459–489.

Kirschke, E., Goswami, D., Southworth, D., Griffin, P.R., and Agard, D.A. (2014). Glucocorticoid receptor function regulated by coordinated action of the Hsp90 and Hsp70 chaperone cycles. Cell *157*, 1685–1697.

Krukenberg, K.A., Southworth, D.R., Street, T.O., and Agard, D.A. (2009). pH-dependent conformational changes in bacterial Hsp90 reveal a grp94-like conformation at pH 6 that is highly active in suppression of citrate synthase aggregation. J. Mol. Biol. *390*, 278–291.

Li, I.T.S., and Walker, G.C. (2011). Signature of hydrophobic hydration in a single polymer. Prod. Natl. Acad. Sci. USA *108*, 16527–16532.

Lorenz, O.R., Freiburger, L., Rutz, D.A., Krause, M., Zierer, B.K., Alvira, S., Cuellar, J., Valpuesta, J.M., Madl, T., Sattler, M., et al. (2014). Modulation of the Hsp90 chaperone cycle by a stringent client protein. Mol. Cell *53*, 941–953.

Marko, J.F., and Siggia, E.D. (1995). Stretching DNA. Macromolecules *28*, 8759–8770.

Mashaghi, A., Bezrukavnikov, S., Minde, D.P., Wentink, A.S., Kityk, R., Zachmann-Brand, B., Mayer, M.P., Kramer, G., Bukau, B., and Tans, S.J. (2016). Alternative modes of client binding enable functional plasticity of Hsp70. Nature *539*, 448–451.

Mashaghi, A., Kramer, G., Bechtluft, P., Zachmann-Brand, B., Driessen, A.J., Bukau, B., and Tans, S.J. (2013). Reshaping of the conformational search of a protein by the chaperone trigger factor. Nature *500*, 98–101.

Mashaghi, A., Mashaghi, S., and Tans, S.J. (2014). Misfolding of luciferase at the single-molecule level. Angew Chem Int Edit *53*, 10390–10393.

Mayer, M.P., and Le Breton, L. (2015). Hsp90: breaking the symmetry. Mol. Cell *58*, 8–20.

Mickler, M., Hessling, M., Ratzke, C., Buchner, J., and Hugel, T. (2009). The large conformational changes of Hsp90 are only weakly coupled to ATP hydrolysis. Nat. Struct. Mol. Biol. *16*, 281–286.

Moayed, F., Bezrukavnikov, S., Naqvi, M.M., Groitl, B., Cremers, C.M., Kramer, G., Ghosh, K., Jakob, U., and Tans, S.J. (2020). The anti-aggregation holdase Hsp33 promotes the formation of folded protein structures. Biophys. J. *118*, 85–95.

Moayed, F., Mashaghi, A., and Tans, S.J. (2013). A polypeptide-DNA hybrid with selective linking capability applied to single molecule nano-mechanical measurements using optical tweezers. PLoS One *8*.

Moran Luengo, T., Kityk, R., Mayer, M.P., and Rudiger, S.G.D. (2018). Hsp90 breaks the deadlock of the Hsp70 chaperone system. Mol. Cell *70*, 545–552.e549.

Morishima, Y., Murphy, P.J.M., Li, D.P., Sanchez, E.R., and Pratt, W.B. (2000). Stepwise assembly of a glucocorticoid receptor center dot hsp90 heterocomplex resolves two sequential ATP-dependent events involving first hsp70 and then hsp90 in opening of the steroid binding pocket. J. Biol. Chem. *275*, 18054–18060.

Mossa, A., de Lorenzo, S., Huguet, J.M., and Ritort, F. (2009). Measurement of work in single-molecule pulling experiments. J. Chem. Phys. *130*.

Motojima-Miyazaki, Y., Yoshida, M., and Motojima, F. (2010). Ribosomal protein L2 associates with E. coli HtpG and activates its ATPase activity. Biochem Bioph Res. Co *400*, 241–245.

Naqvi, M.M., Avellaneda, M.J., Roth, A., Koers, E.J., Roland, A., Sunderlikova, V., Kramer, G., Rye, H.S., and Tans, S.J. (2022). Protein chain collapse modulation and folding stimulation by GroEL-ES. Sci. Adv. *8*, eabl6293.

Nguyen, M.T.N., Knieß, R.A., Daturpalli, S., Le Breton, L., Ke, X., Chen, X., and Mayer, M.P. (2017). Isoform-specific phosphorylation in human Hsp90β affects interaction with clients and the cochaperone Cdc37. J. Mol. Biol. *429*, 732–752.

Nørrelykke, S.F., and Flyvbjerg, H. (2010). Power spectrum analysis with least-squares fitting: amplitude bias and its elimination, with application to optical tweezers and atomic force microscope cantilevers. Rev. Sci. Instrum. *81*, 075103.

Perales-Calvo, J., Giganti, D., Stirnemann, G., and Garcia-Manyes, S. (2018). The force-dependent mechanism of DnaK-mediated mechanical folding. Sci. Adv. *4*, eaaq0243.

Popp, M.W., Antos, J.M., Grotenbreg, G.M., Spooner, E., and Ploegh, H.L. (2007). Sortagging: a versatile method for protein labeling. Nat. Chem. Biol. *3*, 707–708.

Prodromou, C., Roe, S.M., O'Brien, R., Ladbury, J.E., Piper, P.W., and Pearl, L.H. (1997). Identification and structural characterization of the ATP/ADP-binding site in the Hsp90 molecular chaperone. Cell *90*, 65–75.

Ratzke, C., Nguyen, M.N., Mayer, M.P., and Hugel, T. (2012). From a ratchet mechanism to random fluctuations evolution of Hsp90's mechanochemical cycle. J. Mol. Biol. *423*, 462–471.

Rodriguez, F., Arsene-Ploetze, F., Rist, W., Rudiger, S., Schneider-Mergener, J., Mayer, M.P., and Bukau, B. (2008). Molecular basis for regulation of the heat shock transcription factor sigma32 by the DnaK and DnaJ chaperones. Mol. Cell *32*, 347–358.

Schneider, C., Sepp-Lorenzino, L., Nimmesgern, E., Ouerfelli, O., Danishefsky, S., Rosen, N., and Hartl, F.U. (1996). Pharmacologic shifting of a balance between protein refolding and degradation mediated by Hsp90. Proc. Natl. Acad. Sci. USA *93*, 14536–14541.

Shank, E.A., Cecconi, C., Dill, J.W., Marqusee, S., and Bustamante, C. (2010). The folding cooperativity of a protein is controlled by its chain topology. Nature *465*, 637–U134.

Sharma, S.K., De los Rios, P., Christen, P., Lustig, A., and Goloubinoff, P. (2010). The kinetic parameters and energy cost of the Hsp70 chaperone as a polypeptide unfoldase. Nat. Chem. Biol. *6*, 914–920.

Shiau, A.K., Harris, S.F., Southworth, D.R., and Agard, D.A. (2006). Structural analysis of E-coli hsp90 reveals dramatic nucleotide-dependent conformational rearrangements. Cell *127*, 329–340.

Singhal, K., Vreede, J., Mashaghi, A., Tans, S.J., and Bolhuis, P.G. (2015). The trigger factor chaperone encapsulates and stabilizes partial folds of substrate proteins. PLoS Comput. Biol. *11*, e1004444.

Street, T.O., Lavery, L.A., and Agard, D.A. (2011). Substrate binding drives large-scale conformational changes in the Hsp90 molecular chaperone. Mol. Cell *42*, 96–105.

Street, T.O., Zeng, X.H., Pellarin, R., Bonomi, M., Sali, A., Kelly, M.J.S., Chu, F.X., and Agard, D.A. (2014). Elucidating the mechanism of substrate recognition by the bacterial Hsp90 molecular chaperone. J. Mol. Biol. *426*, 2393–2404.

Stull, F., Koldewey, P., Humes, J.R., Radford, S.E., and Bardwell, J.C.A. (2016). Substrate protein folds while it is bound to the ATP-independent chaperone Spy. Nat. Struct. Mol. Biol. *23*, 53–58.

Swoboda, M., Henig, J., Cheng, H.M., Brugger, D., Haltrich, D., Plumeré, N., and Schlierf, M. (2012). Enzymatic oxygen scavenging for photostability without ph drop in single-molecule experiments. ACS Nano *6*, 6364–6369.

Taipale, M., Jarosz, D.F., and Lindquist, S. (2010). HSP90 at the hub of protein homeostasis: emerging mechanistic insights. Nat. Rev. Mol. Cell Bio. *11*, 515–528.

Thomas, J.G., and Baneyx, F. (2000). ClpB and HtpG facilitate de novo protein folding in stressed Escherichia coli cells. Mol. Microbiol. *36*, 1360–1370.

Tian, P., and Best, R.B. (2016). Structural determinants of misfolding in multi-domain proteins. PLoS Comput. Biol. *12*, e1004933.

Ungelenk, S., Moayed, F., Ho, C.T., Grousl, T., Scharf, A., Mashaghi, A., Tans, S., Mayer, M.P., Mogk, A., and Bukau, B. (2016). Small heat shock proteins sequester misfolding proteins in near-native conformation for cellular protection and efficient refolding. Nat. Commun. *7*.

Walther, K.A., Grater, F., Dougan, L., Badilla, C.L., Berne, B.J., and Fernandez, J.M. (2007). Signatures of hydrophobic collapse in extended proteins captured with force spectroscopy. Prod. Natl. Acad. Sci. USA *104*, 7916–7921.

Wang, M.D., Yin, H., Landick, R., Gelles, J., and Block, S.M. (1997). Stretching DNA with optical tweezers. Biophys. J. *72*, 1335–1346.

Yin, J., Lin, A.J., Golan, D.E., and Walsh, C.T. (2006). Site-specific protein labeling by Sfp phosphopantetheinyl transferase. Nat. Protoc. *1*, 280–285.

Zierer, B.K., Rubbelke, M., Tippel, F., Madl, T., Schopf, F.H., Rutz, D.A., Richter, K., Sattler, M., and Buchner, J. (2016). Importance of cycle timing for the function of the molecular chaperone Hsp90. Nat. Struct. Mol. Biol. *23*, 1020–1028.

STAR★METHODS

KEY RESOURCES TABLE

REAGENT or RESOURCE	SOURCE	IDENTIFIER
Antibodies		
Anti-c-Myc	Roche	Cat#1667149
Anti-Digoxigenin from sheep	Sigma-Aldrich	Cat#11333089001
Bacterial and virus strains		
E. coli BL21(DE3) (Luci myc-tag, 4MBP)	Mashaghi et al. (2014)	N/A
E. coli T7 express	New England Biolabs	Cat#C2566I
E. coli MC4100 ΔhtpG::kan (HtpG)	Graf et al. (2009)	N/A
E. coli BL21(DE3)Star/pCodonPlus	Invitrogen	N/A
Chemicals, peptides, and recombinant proteins		
Carboxyl-polystyrene Particles	Spherotec	Cat#CP-20-10
Anti-Digoxigenin Coated Polystyrene Particles	Spherotec	Cat#DIGP-20-2
SPHERO^{TM} Neutravidin Coated Particles	Spherotec	Cat#NVP-20-5
GGGC peptide	Proteogenix	N/A
Sfp synthase	New England Biolabs	Cat#P9302
Protino Ni-NTA Agarose	Macherey-Nagel	Cat#745400.25
Sulfo-SMCC	Thermo-Fisher	Cat#A39268
Critical commercial assays		
Polylink protein coupling kit for COOH microparticles	Polysciences	Cat#24350-1
Oligonucleotides		
Amine oligo: [NH2]-CAGGGCTCTCTAGATTGACT	IDT	N/A
CoA oligo: [CoA]-CAGGGCTCTCTAGATTGACT	Biomers	N/A
Dig primer: [DIG]-GA-[DIG]- GCAGAGCGAGGTATG TAGGCGGTGC	Eurofins	N/A
Biotin primer: [BITEG]-GA-[BDT]-[BDT]- GCAGAGC GAGGTATGTAGGCGGTGC	Eurofins	N/A
Phospho primer for initial PCR: [PHO]-CAGGGCTC TCTAGATTGACTTATGTATCCGCTCATGAGACAATAA	Eurofins	N/A
Phospho primer for partial strand resynthesis: [PHO]-TATGTATCCGCTCATGAGACAATAA	Eurofins	N/A
Recombinant DNA		
pHis10-SUMO-Avi-luci-4myc	Mashaghi et al. (2014)	N/A
pHis-10-SUMO-ybbr-luci-ybbr	This paper	N/A
pHtpG-His10	Graf et al. (2009)	N/A
pHtpG^{E34A}-His10	Graf et al. (2009)	N/A
pCA528-His6-Smt3-Hsp90β	Nguyen et al. (2017)	N/A
pHis10-SUMO-Avi-4MBP	Ungelenk et al. (2016)	N/A
pMAL-c2E-Avi-GRLBD_F602S-LPETGG	This paper	N/A
Software and algorithms		
MATLAB code for force-extension data analysis	Naqvi et al. (2022)	https://doi.org/10.5281/zenodo.5772329
Foldometer, python code for force-extension data analysis	Naqvi et al. (2022)	https://doi.org/10.5281/zenodo.5772283

RESOURCE AVAILABILITY

Lead contact
Further information and requests for resources and reagents should be directed to and will be fulfilled by the lead contact, Sander Tans (s.j.tans@tudelft.nl).

Materials availability
Plasmids generated in this study are available upon request without restrictions.

Data and code availability
- All data reported in this paper is available from the lead contact upon request.
- This paper does not report original code.
- Any additional information required to reanalyze the data reported in this paper is available from the lead contact upon request.

EXPERIMENTAL MODEL AND SUBJECT DETAILS

For the expression of avi-luci-4myc and 4MBP, E. coli BL21 (DE3) was used, for ybbR-luci-ybbR and GR-LBD T7 express (New England Biolabs), for HtpG E. coli MC4100 ΔhtpG:kan, for Hsp90β E. coli BL21(DE3)Star/pCodonPlus (Invitrogen). 'Bacteria were grown only for the purpose of protein purification in our assays. Protein production methods are mentioned in the method details.

METHOD DETAILS

Expression and purification of luciferase
Firefly luciferase was expressed and purified as follows (Mashaghi et al., 2014). Avi-luci-4myc was produced as hybrid protein consisting of an Ulp1-cleavable N-terminal His_{10}-SUMO tag followed by an AviTag, luciferase and four consecutive myc-tags at the C-terminus. Overexpression of the Avi-luci-4myc-encoding gene was performed in *E. coli* BL21(DE3) cells harboring the BirA encoding plasmid pBirAcm (Avidity, LCC, Aurora, Colorado, USA) in LB medium supplemented with 20 mg/L Biotin, 20 mg/L Kanamycin, 10 mg/L Chloramphenicol, 0.1 mM IPTG at 20°C for about 20 h. Cells from 1.5 L culture volume were lysed in buffer L containing 50 mM $NaPO_4$ pH 8, 0.3 M NaCl, 10% glycerol, 2 mM β-mercaptoethanol. The lysate was cleared from cell debris by centrifugation at 35.000 g for 30 min and incubated for 1 h with 2 g Ni-IDA matrix (Protino; Macherey-Nagel, Düren, Germany). The matrix was washed extensively with buffer L and bound protein was eluted in buffer L containing 250 mM imidazole. Eluate fractions containing the hybrid protein were pooled, His_6-Ulp1 protease was added and dialyzed overnight at 4°C in buffer L. The next day, the protein mixture was subjected to a second Ni-IDA purification to remove the His-tagged protease and the His_{10}-SUMO fragment and flow-through fractions containing purified Avi-luci-4myc were concentrated using Vivaspin concentration columns (Vivaproducts, Inc. Littleton, MA).

Complementary to the Avi-luci-4myc hybrid, an additional construct was produced in which Luciferase is flanked on both sides with the ybbR sequence (Yin et al., 2006). Overexpression was done in T7 express cells. The cultures were grown at 30°C to OD_{600} = 0.6 and expression was induced with 0.4 mM IPTG at 18°C for 20 h. Cells were lysed with a microfluidizer (EmulsiFlex-C3, Avestin) in lysis buffer L. The lysate was clarified by centrifugation (95000 g, 1h) and incubated with Ni-IDA matrix (Protino, Machery-Nagel) for 1 h. After incubation, the matrix was washed with buffer L with 10 mM or 20 mM imidazole added and eluted with 250 mM imidazole.

Expression and purification of HtpG
HtpG and HtpG^{E34A} were expressed as C-terminal His_{10}-fusions (Graf et al., 2009) in E. coli MC4100 ΔhtpG:kan, and purified by Ni-IDA-chromatography (Protino, Macherey-Nagel) and anion-exchange chromatography (Resource^{TM} Q, GE Healthcare). The purified proteins were checked to be nucleotide-free by anion-exchange chromatography (Resource^{TM} Q) and by UV detection by 254 nm.

Expression and purification of human Hsp90β
Human Hsp90β was produced from the bacterial expression vector pCA528 (Andreasson et al., 2008) as fusion proteins with an N-terminal His6-Smt3 tag (Nguyen et al., 2017) in the *E. coli* strain BL21(DE3)Star/pCodonPlus (Invitrogen). The cultures were grown to OD_{600} = 0.8–1.0 and expression was induced with 0.5 mM IPTG at 25°C overnight. Cells were lysed by a microfluidizer (EmulsiFlex-C5, Avestin) in lysis buffer A (40 mM HEPES/KOH pH 7.5, 100 mM KCl, 5 mM MgCl2, 10% glycerol, 4 mM β-mercaptoethanol) and 5 mM PMSF, 1 mM Pepstatin A, 1 mM Leupeptin and 1 mM Aprotinin. The lysate first was clarified by centrifugation (30,000 g for 30 min), and then incubated with Ni-IDA matrix (Protino, Macherey-Nagel) for 30 min. After incubation, the matrix was washed with buffer A and bound protein eluted with buffer A containing 250 mM imidazole. The eluted fusion proteins were supplemented with Ulp1 protease, which cleaved the His_6-Smt3 tag, and the mixture was dialyzed overnight against buffer A containing 20 mM KCl. Cleaved recombinant proteins were recovered in the flow-through fractions after a second incubation with Ni-IDA matrix whereas the N-terminal His6-Smt3 tag and Ulp1 remained on the column. Proteins were further purified by anion-exchange chromatography (Resource^{TM} Q; GE Healthcare) with a linear gradient of 0.02–1 M KCl, fractions of eluted proteins were subjected to Superdex 200 16/60 Prep grade column in storage buffer (40 mM HEPES/KOH, pH 7.5, 50 mM KCl, 5 mM MgCl2, 10% glycerol, 4 mM β-mercaptoethanol). The purity and molecular mass were verified by SDS–PAGE and HPLC-electrospray mass spectrometry, confirming the correct primary sequence containing only the N-terminal start-methionine.

Expression and purification of 4MBP

N-terminally biotinylated 4MBP C-terminally fused with 4 Myc tag sequences were produced in *E. coli* BL21(DE3) as hybrid proteins consisting of an N-terminal Ulp1-cleavable N-terminal His$_{10}$-SUMO sequence followed by an AviTag sequence (Avidity, LCC, Aurora, Colorado, USA), facilitating *in vivo* biotinylation and four consecutive C-terminal Myc-tag sequences (Ungelenk et al., 2016). Proteins were purified from *E. coli* BL21(DE3) cells harboring pBirAcm encoding the biotin ligase (Avidity, LCC, Aurora, Colorado, USA). For over-expression cells over-night cultures were diluted 1:100 in fresh LB medium supplemented with 20 mg/L Biotin, 20 mg/L Kanamycin, 10 mg/L Chloramphenicol, 0.2% glucose and incubated under vigorous shaking at 30°C. Expression was induced at OD_{600} = 0.6 by addition of 1 mM IPTG for 3 h. Cells were chilled, harvested by centrifugation, flash-frozen in liquid nitrogen and stored at −70°C. Cell pellets were resuspended in ice-cold buffer A (20 mM Tris-HCl pH 7.5, 0.2 M NaCl, 1% Triton X-100, 1 mM PMSF) and lysed using a French Pressure Cell. The lysate was cleared from cell debris by centrifugation at 35.000 g for 30 min and incubated with Ni-IDA matrix (Protino; Macherey-Nagel, Düren, Germany) for 30 min at 4°C. The matrix was washed extensively with buffer A and bound hybrid proteins were eluted in buffer A containing 250 mM imidazole. The eluate was supplemented with His$_6$-Ulp1 protease and dialyzed overnight at 4°C in buffer D (20 mM Tris-HCl pH 7.5, 0.2 M NaCl). Following dialysis coupled with Ulp1 digestion, His$_6$−Ulp1 protease and the His$_{10}$−SUMO fragment were removed by incubation with Ni-IDA matrix. The unbound MBP or 4 MBP that remained in the unbound fraction was then loaded on Amylose resin (New England Biolabs) previously equilibrated in buffer D, washed with cold buffer D and bound proteins were eluted in buffer D supplemented with 20 mM maltose. Elution fractions were dialyzed three times for 2 h at 4°C in 100-fold excess volume of buffer S (20 mM Tris-HCl pH 7.5, 0.2 M NaCl, 1 mM EDTA). 4 MBP purifications in addition were subjected to size-exclusion chromatography using a Superdex 200 HiLoad 16/60 prep grade column. Purified proteins were concentrated using Vivaspin centrifugal concentrators, aliquoted, flash frozen in liquid nitrogen and stored at −70°C.

Expression and purification of GRLBD

Human GRLBD-F602S (520-778), flanked with an AviTag (Beckett et al., 2008) on the N-terminal side and a Sortag (Popp et al., 2007) on the C-terminus, was produced in *E. coli* T7 express (New England Biolabs) as an MBP fusion in the pMAL-c2E vector in the presence of 100 μg/L Ampicillin, 17 μg/L Chloramphenicol, 20 mg/L D-biotin and 50 μM dexamethasone (Sigma-Aldrich). The protein was in-vivo biotinylated using BirA produced from the pBirAcm plasmid (Avidity LCC, Aurora, CO, USA). Expression of the GRLBD-encoding gene was induced with 0.5 mM IPTG at 15°C for 16 h. The cells where harvested by centrifugation 4°C, 5000 g, dissolved in lysis buffer (wash buffer without ATP and with complete protease inhibitor cocktail (Roche) 20 min, and lysed using Emulsiflex C3 homogenizer (Avestin, Ottawa, Canada). Insoluble material was removed by ultracentrifugation at 100,000 g for 1h at 4°C. The lysate was affinity purified using amylose resin (New England Biolabs, Ipswich, MA, USA). Wash buffer was 50 mM Tris pH 8.3, 300 mM KCl, 5 mM MgCl$_2$, 0.04% CHAPS, 1 mM EDTA, 10% glycerol, 50 μM dexamethasone, 2 mM ATP and 5 mM β-mercaptoethanol. GR-LBD was eluted with wash buffer supplemented with 10 mM D-Maltose. Using a PD-10 desalting column (GE healthcare) buffer was exchanged to storage buffer (50 mM Tris pH 8.3, 100 mM KCl, 5 mM MgCl$_2$, 10% glycerol, 50 μM dexamethasone and 5 mM β-mercaptoethanol).

Coupling of oligos to GRLBD

5'NH2-labeled CAGGGCTCTCTAGATTGACT (IDT-DNA, Leuven, Belgium) was coupled with sulfo-SMCC (Thermo-Fisher) according to the manufacturer's instructions resulting in a maleimide-labeled oligo. The product was purified by ethanol precipitation. A GlyGlyGlyCys peptide (Proteogenix, Schiltigheim, France), was dissolved in MeOH to 10 mM and added in a 6:1 ratio to 300 μM oligo-maleimide and incubated for 1h at 37°C. To drive the reaction to completion, 0.5 mM TCEP was added and the reaction mixture was incubated for 30 min at 37°C. The reaction was stopped by addition of 0.1 M sodium molybdate (Kalia and Raines, 2007). The product purified by 2 ethanol-precipitation steps. The glycine-modified oligo is coupled to the GR using the Sortase A reaction (Antos et al., 2017). 7M Sortase A was expressed in *E. coli* from pet30b-7M SrtA (Addgene plasmid #51141 was a gift from Hidde Ploegh) and purified according to Popp et al. (Antos et al., 2017). In order to remove the non-reacted glycine-modified oligo, a second affinity (amylose) purification was performed.

Coupling of oligos to luciferase

The oligo, 5'- labeled with Coenzyme A (Biomers GmbH), SFP synthase (New England Biolabs) and purified ybbR-Luciferase-ybbR were incubated over night at 4°C. A second His-tag purification was done to remove the non-reacted Coenzyme A-modified oligo.

Coupling of DNA tether to GR-oligo and luciferase-oligo

A 2.5 kbp DNA fragment was PCR amplified from the pUC19 plasmid (New England Biolabs) with a double digoxigenin-labeled primer (Biomers GmbH) or triple biotin-labeled primer on one side and a phosphoprimer on the other side and purified using the QIAquick PCR purification kit (Qiagen, Hilden, Germany). The phosphorylated strand is digested by Lambda exonuclease (New England Biolabs) for 2 h at 37°C and purified using an Amicon 30 kDa MWCO filter (Merck, Darmstadt, Germany). The Deep Vent exo- DNA polymerase (New England Biolabs) and a primer missing the first 5′ nucleotides compared to the phosphoprimer used for the PCR is used for the fill up of the second DNA strand creating a 20 nt overhang. This overhang is complementary to the 20 nt oligonucleotide sequence

ligated to the C-terminus of GRLBD and N- and C-terminus of Luciferase. The overhang DNA is added to the GR-oligo or Luciferase-oligo together with T4 ligase (New England Biolabs) and incubated for 30 min at 16°C followed by 30 min on ice. The resulting hybrid was measured directly or flash frozen and stored at −80°C until measurement.

Coupling of DNA tether to luciferase-oligo
A similar procedure was used for attaching two long DNA handles two ybbR-Luciferase-ybbR as for the GR-oligo. For this reaction, half of the DNA was a biotin labeled and the other half contained the (previously described) digoxigenin-labeled DNA. The biotin labeled DNA handles were made in the same way was as digoxigenin-labed DNA, but instead of a digoxigenin primer, a triple-labeled biotin primer (Biomers GmbH) was used.

Bead preparation luciferase and 4MBP
We used commercially provided AntiDig-coated beads (Spherotech, 2μm diameter), Neutravidin-coated bead (Spherotec, 2.1 μm diameter) and prepared the AntiMyc-coated beads in-house. Anti-c-Myc (Roche) molecules were covalently linked to the carboxylated polystyrene beads (Spherotech) via Carbodiimide reaction (PolyLink Protein Coupling Kit, Polysciences Inc.). 5 μL of 5% (w/v) 2 μm diameter carboxylated polystyrene microspheres were washed twice by pelleting at 13,200 rpm (for 10 min) in a microcentrifuge tube and resuspending in coupling buffer (400 μL in first wash and 170 μL in second washing) (PolyLink Protein Coupling Kit, Polysciences Inc.). Then 20 μL of the freshly prepared EDCA solution (20 mg/mL; prepared by dissolving 1 mg EDCA in 50 μL coupling buffer) was added to the microparticle suspension and mixed gently end-over-end. After that, 20 μg of Anti-c-Myc was added and the mixture was incubated for 1 h at room temperature with gentle mixing. Then the mixture was washed twice in 400 μL storage buffer. AntiMyc-coated beads were stored in 400 μL storage buffer (containing 0.05% BSA) at 4°C until use.

DNA-coated microspheres were made by mixing ~70 ng of dsDNA molecules and 1 μL AntiDig-coated beads in 10 μL HKM (50 mM HEPES, pH 7.6, 100 mM KCl, 5 mM MgCl$_2$) buffer. After 30 min incubation on a rotary mixer (4°C), 1 μg of Neutravidin was added to the beads solution. Beads were again incubated for 15 min on a rotary mixer (4°C). The unreacted Neutavidin molecules were separated by pelleting the beads at 13,200 rpm (for 10 min) in a microcentrifuge tube. After taking the supernatant, the beads were resuspended in 400 μL HKM buffer for use in optical tweezers experiments.

Protein-coated microspheres were made by mixing ~10 μg of Luciferase molecules and 1 μL AntiMyc-coated beads in 10 μL HKM (50 mM HEPES, pH 7.6, 100 mM KCl, 5 mM MgCl$_2$) buffer. After 30 min incubation on a rotary mixer (4°C), the beads were diluted in 400 μL HKM buffer for use in optical tweezers experiments.

For the ybbR-Luciferase-ybbR construct, the same procedure was used as for GRLBD, except that the measurements were done in HKM buffer.

Bead preparation GRLBD
The GR-DNA chimeras were tethered to the surface of 2.1 μm AntiDig-coated polystyrene beads in HMKDM buffer (50 mM HEPES pH 7.5, 5 mM MgCl$_2$ and 100 mM KCl, 50 uM dexamethasone, 5 mM β-mercaptoethanol). After 40 min incubation on a rotary mixer (4°C), the beads were diluted in 175 μL HMKDM buffer for use in optical tweezers experiments supplemented with an enzymatic oxygen scavenger system (Swoboda et al., 2012). For experiments in the presence of chaperone, the HMKDM supplemented with Hsp90-β (2 μM), ATP (1 mM), phosphoenolpyruvate (3 mM), and pyruvate kinase (20 μg/mL).

Optical tweezers buffer conditions
The MBP and Luciferase experiments were carried out in HMK (50 mM HEPES, pH 7.6, 100 mM KCl, 5 mM MgCl$_2$) buffer, supplemented with HtpG (1 μM), HtpG^{E34A} (5 μM), and ATP (1 mM). The GR experiments were carried out in HMKDM buffer (50 mM HEPES pH 7.5, 5 mM MgCl$_2$ and 100 mM KCl, 50 uM dexamethasone, 5 mM β-mercaptoethanol), supplemented with Hsp90-β (2 μM), ATP (1 mM), phosphoenolpyruvate (3 mM), and pyruvate kinase (20 μg/mL).

Optical tweezer setup
Two optical tweezers set-ups were used. The first is a custom-built single trap optical tweezers (Mashaghi et al., 2013; Moayed et al., 2013). Detection of forces on the trapped bead was performed using back focal plane interferometry. Forces were recorded at 50 Hz. A piezo-nanopositioning stage (Physik Instrumente) was used to move the sample cell and micropipette at a speed of 50 nm s^{-1}. The beads were trapped in a flow chamber with three input channels: one containing AntiMyc-coated beads with the protein construct; one containing AntiDig-coated beads with the DNA linker and a central buffer channel in which the measurements were conducted. The second is a custom-built dual-trap optical tweezers. A single solid-state laser (IPG Photonics, 5 W) was split by polarization into two independently controlled traps. Forces were monitored in both traps separately using back-focal plane interferometry (Gittes and Schmidt, 1998) and bead displacement was calculated according to $\Delta F = -\kappa \Delta y$. The stiffness of the traps was determined by thermal calibration using the power spectrum method (Nørrelykke and Flyvbjerg, 2010). Data was acquired at 195 Hz.

Bulk luciferase refolding assay
In the first step, firefly luciferase (10 uM) was chemically denatured by incubating with unfolding buffer (5 M GdmCl, 30 mM Tris/acetate pH 7.5) for 10 min at room temperature. Afterward the denatured luciferase was diluted 125-fold in refolding buffer (25 mM

HEPES/KOH pH 7.6, 100 mM KOAc, 10 mM Mg(OAc)2, 2 mM ATP, 5 mM DTT) (80 nM final luciferase concentration) in the presence or absence of 20 uM HtpG or/and 2 mM ATP, then incubated at 30°C for 30 min. Then 0.8 uM DnaK, 0.16 uM DnaJ and 0.4 uM GrpE (K:J:E 10:2:5) were added and the reaction further incubated at 30°C. The luciferase activity was measured every 5 min by photon counting in a Lumat LB 9507 (Berthold Technologies) by adding 1 uL of sample into 124 uL of assay buffer (100 mM K-phosphate buffer pH 7.6, 25 mM Glycylglycine, 100 mM KOAc, 15 mM Mg(OAc)2, 5 mM ATP), then mixed with 125uL of 80uM luciferase.

QUANTIFICATION AND STATISTICAL ANALYSIS

Protein length determination

To determine measured protein lengths, we fitted measured force-extension data to a worm-like chain model (Wang et al., 1997) of a DNA-Polypeptide construct, with the polypeptide-contour length (L_p) as the fitting parameter (S1). D and p indexes indicate DNA and polypeptide, respectively.

$$F_{WLC, D}(x) = \frac{k_B T}{p_D}\left(\frac{1}{4}\left(1 - \frac{x_D}{L_D} + \frac{F}{K}\right)^{-2} - \frac{1}{4} + \frac{x_D}{L_p} - \frac{F}{K}\right)$$

Equation S1

$$F_{WLC, p}(x) = \frac{k_B T}{p_p}\left(\frac{1}{4}\left(1 - \frac{x_p}{L_p}\right)^{-2} - \frac{1}{4} + \frac{x_p}{L_p}\right)$$

Here, F is the force, x is the extension (end-to-end distance), L is the contour length, p is the persistence length, K is the stretch modulus, k_B is the Boltzmann constant, and T is absolute temperature. The force-extension data was fitted considering the DNA linker and the polypeptide as two springs in series, i.e. $F = F_{WLC,D} = F_{WLC,p}$; $x_{Total} = x_D + x_p$. We note the protein length is assumed to be equal to the contour length of the unfolded part of the protein chain, given the comparatively small contribution of folded structures to the measured length. Worm-like-chain parameters used in this study are the following: For the MBP and Luciferase-Myc experiments, K_D = 1200 pN, p_D = 45 nm, p_P = 1 nm, L_P (luciferase) = 198 nm, L_P (4MBP) = 480 nm, L_D = 920 nm was used. For the luciferase-ybbR experiments: p_D = 20 nm, K_D = 1250 pN, p_P = 0.75 nm, L_P = 187 nm, L_D = 906 nm. For the GRLBD measurements: p_D = 20 nm, K_D = 1200 pN, p_P = 0.75 nm, L_P = 95 nm, L_D = 906 nm was used.

Analysis of force-extension data

Before taking data on a particular tether, we performed several controls to confirm only a single tether is present. We check that the total unfolding of the proper expected length, and that the force-extension data is consistent with the WLC model (at higher forces). We also monitor that the tethers overstretch at 65 pN. At the end of experimentation on a tether, we check that it breaks in one clean break. For the analysis of Figures 1E, 3C, and 4C, we followed previous work on the folding and unfolding of Luciferase alone (Mashaghi et al., 2014), which showed that the smallest partially refolded state of Luciferase unfolded with a contour length change of 31 nm. We divided the relax-stretch cycles into two categories: stretching curves that showed contour-length changes of less than 31 nm in total above 5pN (and hence have remained predominantly unfolded, light blue (or gray) bars Figures 1E and 4C), and those showing contour length changes of more than 31 nm above 5 pN (dark blue (or gray) bars Figures 1E and 4C). We observed chains that for a number of cycles did not refold, and then again refolded. This longer-term memory could be due to slow proline isomerization or residue rotational angle relaxation. There is the added possibility that HtpG remains associated, which can also lead to memory. The relaxation energy (Figures 2E, 4B, S1A, S1C and S1E) refers to the surface area in between an experimental force-extension curve during relaxation, and the theoretical WLC force-extension curve for the DNA tether connected to a polypeptide of appropriate length (Equation S1) (Mossa et al., 2009). Similarly, we refer to the stretching energy (Figure 2G) as the surface area in between an experimental force-extension curve during stretching, and the theoretical WLC force-extension curve for the DNA tether connected to a polypeptide of appropriate length.

The MATLAB and Python codes used for the analysis are available online (https://doi.org/10.5281/zenodo.5772329 and https://doi.org/10.5281/zenodo.5772283, respectively), previously reported in (Naqvi et al., 2022)

The N-values of the experiments represent separate stretch- or relaxation curves or full cycles and for each figure are reported in the figure captions. Statistical significance was determined using two-sided student t-test and are reported in the results section, error bars in Figures 1E, 3C, 4B, 4C and S3A are SEM and in Figures S3D SD.